

1 **Oceanic bromine bromoform emissions weighted by their ozone depletion**
2 **potential**

3
4
5 **S. Tegtmeier¹, F. Ziska¹, I. Pisso², B. Quack¹, G. J. M. Velders³, X. Yang⁴, and K.**
6 **Krüger⁵**

7
8
9 ¹GEOMAR Helmholtz Centre for Ocean Research Kiel, Kiel, Germany

10
11 ²Norwegian Institute for Air Research (NILU), Kjeller, Norway

12
13 ³National Institute for Public Health and the Environment, Bilthoven, the Netherlands

14
15 ⁴British Antarctic Survey, Cambridge, UK

16
17 ⁵University of Oslo, Oslo, Norway

18
19
20
21
22
23
24
25
26
27
28
29
30
31
32 To be submitted to Atmospheric Chemistry and Physics

33 **Abstract**

34

35 ~~At present, anthropogenic halogens and oceanic emissions of Very Short-Lived Substances~~
36 ~~(VSLs) are responsible for stratospheric ozone destruction. Emissions of the, mostly long-~~
37 ~~lived, anthropogenic halogens have been reduced, and as a consequence, their atmospheric~~
38 ~~abundance has started to decline since the beginning of the 21st century. Emissions of VSLs~~
39 ~~are, on the other hand, expected to increase in the future. VSLs are known to have large~~
40 ~~natural sources; however increasing evidence arises that their oceanic production and~~
41 ~~emission is enhanced by anthropogenic activities. **At present, anthropogenic halogens and**~~
42 **oceanic emissions of Very Short-Lived Substances (VSLs) both contribute to the**
43 **observed stratospheric ozone depletion. Emissions of the long-lived anthropogenic**
44 **halogens have been reduced and are currently declining, whereas emissions of the**
45 **biogenic VSLs are expected to increase in future climate due to anthropogenic activities**
46 **affecting oceanic production and emissions.** Here, we introduce a new approach of
47 assessing the impact of oceanic halocarbons on stratospheric ozone by calculating their Ozone
48 Depletion Potential (ODP)-weighted emissions. Seasonally and spatially dependent, global
49 distributions are derived **within a case-study framework** for CHBr_3 for the period 1999 -
50 2006. At present, ODP-weighted emissions of CHBr_3 amount up to 50% of ODP-weighted
51 anthropogenic emissions of CFC-11 and to 9% of all long-lived ozone depleting halogens.
52 The ODP-weighted emissions are large where strong oceanic emissions coincide with high-
53 reaching convective activity and show pronounced peaks at the equator and the coasts with
54 largest contributions from the Maritime Continent and West Pacific. Variations of tropical
55 convective activity lead to seasonal shifts in the spatial distribution of the ODP with the
56 updraught mass flux explaining 71% of the variance of the ODP distribution. Future climate
57 projections based on the RCP 8.5 scenario suggest a 31% increase of the ODP-weighted
58 CHBr_3 emissions until 2100 compared to present values. This increase is related to a larger
59 convective activity **updraught mass flux in the upper troposphere** and increasing
60 emissions in a future climate. However, at the same time, it is reduced by less effective
61 bromine-related ozone depletion **coupled to declining stratospheric chlorine**
62 **concentrations.** The comparison of the ODP-weighted emissions of short and long-lived
63 halocarbons provides a new concept for assessing the overall impact of oceanic halocarbon
64 emissions on stratospheric ozone depletion for current conditions and future projections.

65

66 **1 Introduction**

67

68 The overall abundance of ozone-depleting substances in the atmosphere has been decreasing
69 since the beginning of the 21 century as a result of the successful implementation of the 1987
70 Montreal Protocol and its later Adjustments and Amendments (Montzka et al., 2011). In
71 contrast to the long-lived halocarbons, the halogenated Very Short-Lived Substances (VSLS)
72 with chemical lifetimes of less than 6 months are not controlled by the Montreal Protocol and
73 are even suggested to increase in the future (Hepach et al., 2014; **Hossaini et al., 2015**).
74 Brominated VSLS are known to have large natural sources; however evidence arises that their
75 oceanic production and emissions are enhanced through anthropogenic activities which are
76 expected to increase in the future (Leedham et al., 2013; Ziska et al., in prep.). At present,
77 oceanic VSLS provide a significant contribution to the stratospheric bromine budget
78 (**Carpenter and Reimann et al., 2014**). In the future, the decline of anthropogenic chlorine
79 and bromine will further increase the relative impact of oceanic VSLS on stratospheric
80 chemistry. The absolute amount of bromine-related ozone loss, on the other hand, is expected
81 to decrease due to decreasing stratospheric chlorine concentrations and thus a less efficient
82 BrO/ClO ozone loss cycle (Yang et al., 2014). Furthermore, the impacts of climate change on
83 surface emissions, troposphere-stratosphere transport, stratospheric chemistry and residence
84 time will change the role of VSLS (Pyle et al., 2007; Hossaini et al., 2012). While
85 stratospheric ozone depletion due to long-lived halocarbons is expected to level off and
86 reverse (Austin and Butchart, 2003), it remains an important challenge to assess the role of
87 oceanic VSLS on stratospheric ozone in a future changing climate.

88

89 Over the last years there has been increasing evidence from observational (e.g., Dorf et al.,
90 2006, Sioris et al., 2006) and modelling (e.g., Warwick et al. 2006, Liang et al., 2010;
91 Tegtmeier et al., 2012) studies that VSLS provide a significant contribution to stratospheric
92 total bromine (Br_y). Previous estimates ranging between 1 and 8 ppt (Montzka et al., 2011)
93 recently seem to converge to a slightly narrower range including observation-derived
94 estimates of 2.9 ppt (Sala et al., 2014) and model-derived estimates of 4 ppt (Hossaini et al.,
95 2013), 4.5-6 ppt (Aschmann and Sinnhuber, 2013) and 7.7 ppt (Liang et al., 2014).
96 **Brominated VSLS reduce ozone in the lower stratosphere with current estimates of a 3-**
97 **11% contribution to ozone depletion (Hossaini et al., 2015) or a 2-10% contribution**
98 **(Braesicke et al., 2013; Yang et al., 2014). Through the relatively large impact of VSLS**

99 **on ozone in the lower stratosphere they have a radiative effect corresponding to a**
100 **contribution of -0.02 W m^{-2} to global radiative forcing (Hossaini et al., 2015).**

101
102 The most abundant bromine containing VSLS are dibromomethane (CH_2Br_2) and bromoform
103 (CHBr_3) with potentially important source regions in tropical, subtropical and shelf waters
104 (Quack et al., 2007). The contribution of VSLS to stratospheric bromine in form of organic
105 source gases or inorganic product gases depends strongly on the efficiency of troposphere-
106 stratosphere transport compared to the photochemical loss of the source gases and to the wet
107 deposition of the product gases. Uncertainties in the contribution of VSLS to stratospheric
108 halogen loading mainly result from uncertainties in the emission inventories (e.g., Hossaini et
109 al., 2013) and from uncertainties in the modeled transport and wet deposition processes (e.g.,
110 Schofield et al., 2011).

111
112 The relative contribution of individual halocarbons to stratospheric ozone depletion is often
113 quantified by the Ozone Depletion Potential (ODP) defined as the time-integrated ozone
114 depletion resulting from a unit mass emission of that substance relative to the ozone depletion
115 resulting from a unit mass emission of CFC-11 (CCl_3F) (Wuebbles, 1983). ~~Ozone depletion~~
116 ~~and thus the definition of the ODP refer to anthropogenically emitted halogens.~~ Independent
117 of the total amount of the substance emitted, the ODP describes only the potential but not the
118 actual damaging effect of the substance to the ozone layer, relative to that of CFC-11. While
119 the ODP, **traditionally defined for anthropogenic**, long-lived halogens, is a well-
120 established and extensively used measure and plays an important role in the Montreal
121 Protocol for control measures and reporting of emissions. ~~, the same concept can not easily be~~
122 ~~applied to shorter lived substances. The ODP is traditionally defined for anthropogenic, long-~~
123 ~~lived halogens. However,~~ Some recent studies have applied the ODP concept to VSLS (e.g.,
124 Brioude et al., 2010; Pisso et al., 2010), which have also natural sources. Depending on the
125 meteorological conditions, only fractions of the originally released VSLS reach the
126 stratosphere. As a consequence the ODP of a VSLS cannot be given as one number as for the
127 long-lived halocarbons but needs to be quantified as a function of time and location of
128 emission. So far ODPs of VSLS have been estimated based on Eulerian (Wuebbles et al.,
129 2001) and Lagrangian (Brioude et al., 2010; Pisso et al., 2010) studies, showing strong
130 geographical and seasonal variations, in particular within the tropics. The studies
131 demonstrated that the ODPs of VSLS are to a large degree determined by the efficiency of

132 vertical transport from the surface to the stratosphere and that uncertainties in the ODPs arise
133 mainly from uncertainties associated with the representation of convection.

134

135 Combining the emission strength and the ozone-destroying capabilities of a substance in a
136 meaningful way can be achieved by calculating the ODP-weighted emissions. For the long-
137 lived halocarbons, global ODP-weighted emissions can be calculated as the product of two
138 numbers, their mean global emissions and their ODPs (e.g., Velders et al., 2007;
139 Ravishankara et al., 2009). For the VSLS, however, the concept of ODP-weighted emissions
140 has not been applied yet and will require weighting the spatially and temporally highly
141 variable emissions with the also highly variable ODPs. Among the brominated VSLS, the
142 calculation of CHBr_3 ODP-weighted emissions is now possible since global emission
143 inventories (Ziska et al., 2013) and global ODP maps (Pisso et al., 2010) became available.
144 ODP-weighted emissions will provide insight in where and when the CHBr_3 is emitted that
145 impact stratospheric ozone. Furthermore, in a globally averaged framework the ODP-
146 weighted emissions will allow to compare the impact of past, present and future long- and
147 short-lived halocarbon emissions. The ODP-weighted emissions for the anthropogenic
148 component of the CHBr_3 emission budget cannot be calculated, since no reliable estimates of
149 anthropogenic contributions are available at the moment. The concept is introduced here for
150 the available total emission inventory.

151

152 We compile ODP-weighted emissions of CHBr_3 in form of the seasonal and annual mean
153 distribution in order to assess the overall impact of oceanic CHBr_3 emissions on stratospheric
154 ozone. First, we introduce the new approach of calculating ODP-weighted VSLS emissions,
155 which takes into account the high spatial variability of oceanic emission and ODP fields
156 (Section 2). Maps and global mean values of ODP-weighted CHBr_3 emissions for present day
157 conditions are given in Section 3. The method and application are introduced for CHBr_3 ,
158 within a case-study framework and can be applied to all VSLS where emissions and ODP are
159 available at a spatial resolution necessary to describe their variability. In Section 4, we
160 demonstrate that ODP fields of short-lived gases can be estimated based on the convective
161 mass flux from meteorological reanalysis data and develop a proxy for the ODP of CHBr_3 .
162 We use this method to derive long-term time series of ODP-weighted CHBr_3 emissions for
163 1979-2013 based on ERA-Interim data in Section 5. Model-derived ODP-weighted CHBr_3
164 emissions for present conditions are introduced in Section 6. Based on model projections of
165 climate scenarios, the future development of the ODP-weighted CHBr_3 emissions is analyzed

166 in Section 7. This approach provides a new tool for an assessment of future growing biogenic
167 VSLS and declining chlorine emissions in form of a direct comparison of the global-averaged
168 ODP-weighted emissions of short- and long-lived halocarbons.

169

170 **2 Data and methods**

171

172 **2.1 CHBr₃ emissions**

173

174 The present-day global emission scenario from Ziska et al. (2013) is a bottom-up estimate of
175 the oceanic CHBr₃ fluxes. Emissions are estimated using global surface concentration maps
176 generated from the atmospheric and oceanic in-situ measurements of the HalOcAt
177 (Halocarbons in the ocean and atmosphere) database project (<https://halocat.geomar.de>). The
178 in-situ measurements collected between 1989 and 2011 were classified based on physical and
179 biogeochemical characteristics of the ocean and atmosphere and extrapolated to a global
180 1°x1° grid with the Ordinary Least Square regression technique. Based on the concentration
181 maps, the oceanic emissions were calculated with the transfer coefficient parameterization of
182 Nightingale et al. (2000) adapted to CHBr₃ (Quack and Wallace, 2003). The concentration
183 maps represent climatological fields covering the time period 1989-2011. The emissions are
184 calculated as a 6-hourly time series based on meteorological ERA-Interim data (Dee et al.,
185 2011) for 1979-2013 under the assumption that the constant concentration maps can be
186 applied to the complete time period (Ziska et al., 2013). Recent model studies showed that
187 atmospheric CHBr₃ derived from the Ziska et al. (2013) bottom-up emission inventory agrees
188 better with tropical atmospheric measurements than the other CHBr₃ model estimates derived
189 from top-down emission inventories (Hossaini et al., 2013).

190

191 Future emission estimates are calculated based on the present day (1989-2011) climatological
192 concentration maps and future estimates of global sea surface temperature, pressure, winds
193 and salinity (Ziska et al., **in prep.**). The meteorological parameters are model output from the
194 Community Earth System Model version 1 - Community Atmospheric Model version 5
195 (CESM1-CAM5) (Neale et al., 2010) runs based on the Representative Concentration
196 Pathways (RCP) 8.5 scenarios conducted within phase 5 of the Coupled Model
197 Intercomparison Project (CMIP5) (Taylor et al., 2012). The CESM1-CAM5 model has been
198 chosen since it provides model output for all the parameters required to calculate future VSLS
199 emissions and future ODP estimates (Section 2.2). Comparisons have shown that the global

200 emissions based on historical CESM1-CAM5 meteorological data agree well with emissions
201 based on ERA-Interim fields (Ziska et al., **in prep.**). **For the time period 2006-2100, the**
202 **global monthly mean emissions are calculated based on the monthly mean**
203 **meteorological input parameters from CESM1-CAM5 and the fixed atmospheric and**
204 **oceanic concentrations from Ziska et al. (2013) following the parameterization of air-sea**
205 **gas exchange coefficient from Nightingale et al. (2000).** The future global CHBr₃ emissions
206 increase by about 30% until 2100 for the CESM1-CAM5 RCP 8.5 simulation. These derived
207 changes of the future VSLS emissions are only driven by projected changes in the
208 meteorological and marine surface parameters, **in particular, the by changes in surface**
209 **wind and sea surface temperature. The respective contributions of wind and**
210 **temperature changes to the future emission increase can vary strongly depending on the**
211 **oceanic region (Ziska et al., in prep).** The future emissions do not take into account possible
212 changes of the oceanic concentrations, **since no reliable estimates of future oceanic**
213 **halocarbon production and loss processes exist so far.**

214

215 **2.2 CHBr₃ trajectory-derived ODP**

216

217 The Ozone Depletion Potential is a measure of a substance's destructive effect to the ozone
218 layer relative to the reference substance CFC-11 (CCl₃F). ODPs of long-lived halogen
219 compounds can be calculated based on the change in total ozone per unit mass emission of
220 this compound using atmospheric chemistry-transport models. Alternatively, the ODP of a
221 long lived species *X* can be estimated by a semi-empirical approach (Solomon et al., 1992):

222

$$223 \quad ODP_X = \frac{M_{CFC-11}}{M_X} \frac{\alpha n_{Br} + n_{Cl}}{3} \frac{\tau_X}{\tau_{CFC-11}} \quad (1)$$

224

225 where τ is the global atmospheric lifetime, M is the molecular weight, n is the number of
226 halogen atoms and α is the effectiveness of ozone loss by bromine relative to ozone loss by
227 chlorine. In contrast to the long-lived halocarbons, for VSLS the tropospheric transport time
228 scale plays a dominant role for the calculation of their ODP and the concept of a global
229 lifetime τ_X cannot be adapted. Therefore, the global lifetime needs to be replaced by an
230 expression weighting the fraction of VSLS reaching the tropopause and their subsequent
231 residence time in the stratosphere.

232

233 Following a method previously developed specifically for VSLS, the ODP of CHBr_3 is
234 calculated as a function of location and time of emission (x_e, t_e) based on ERA-Interim
235 driven FLEXPART trajectories (Pisso et. al., 2010). Based on the trajectory calculations, the
236 fraction of VSLS reaching the tropopause and the stratospheric residence time are derived.
237 Owing to the different timescales and processes in the troposphere and stratosphere, the
238 estimates are based on separate ensembles of trajectories quantifying the transport in both
239 regions. The tropospheric trajectory ensembles are used to determine the fraction of VSLS
240 reaching the tropopause at different injection points (y, s) . The subsequent residence time in
241 the stratosphere is quantified from stratospheric trajectories ensembles run for a longer time
242 period (20 years). ODPs as a function of location and time of emission were obtained from
243 equation (1) where the expression $\int_{t_e}^{\infty} \int_{\Omega} \sigma r_X^{\Omega} T^{strat} dy ds$ replaces τ_X . This expression
244 integrated in time s starting at the emission time t_e and throughout the surface Ω (representing
245 the tropopause) is estimated from the tropospheric and stratospheric trajectory ensembles.
246 Tropospheric transport appears as the probability $\sigma(y, s; x_e, t_e)$ of injection at (y, s) in Ω
247 while physico-chemical processes in the troposphere appear as the injected proportion of total
248 halogen emitted $r_X^{\Omega}(y, s; x_e, t_e)$. Stratospheric transport is taken into account by $T^{strat}(y, s)$
249 which expresses the stratospheric residence time of a parcel injected at the tropopause at
250 (y, s) . An ozone depletion efficiency factor of 60 is used for bromine (Sinnhuber et al., 2009).
251 A more detailed derivation of the approximations and parameterizations including a
252 discussion of the errors involved can be found in Piss0 et al. (2010).

253

254 **2.3 CHBr_3 mass flux-derived ODP**

255

256 While present day ODP estimates for VSLS based on ERA-Interim are available (e.g., Piss0
257 et al., 2010), the trajectory-based method has not been applied to future model scenarios so
258 far. Therefore, we attempt to determine an ODP proxy easily available from climate model
259 output, which can be used to derive future estimates of the ODP fields. In general, the ODP of
260 a VSLS as a function of time and location of emission is determined by tropospheric and
261 stratospheric chemistry and transport processes. It has been shown, however, that the effect of
262 spatial variations in the stratospheric residence time on the ODP is relatively weak (Piss0 et
263 al., 2010). We identify a pronounced relationship between the ODP of CHBr_3 and deep
264 convective activity, which demonstrates that for such short-lived substances the ODP
265 variability is mostly determined by tropospheric transport processes. Based on the identified
266 relationship we develop a proxy for the ODP of CHBr_3 based on the ERA-Interim convective

267 upward mass flux. For the available trajectory-derived ODP fields, we determine a linear fit
268 $[a_0, a_1]$ with residual r in a least-square sense:

$$269 \quad y = a_0 + a_1x + r. \quad (2)$$

270
271 The dependent variable y is the trajectory-based ODP prescribed as a vector of all available
272 monthly mean ODP values comprising 26 months of data re-gridded to the ERA-Interim
273 standard resolution of $1^\circ \times 1^\circ$. The independent variable x is a vector of the ERA-Interim
274 monthly mean updraught mass flux between 250 and 80 hPa with a $1^\circ \times 1^\circ$ resolution for the
275 same months. The fit coefficients $[a_0, a_1]$ are used to calculate the ODP proxy \hat{y}

$$277 \quad \hat{y} = a_0 + a_1x. \quad (3)$$

278
279 The fit scores a coefficient of determination of $r^2 = 0.71$ conveying that our ODP proxy
280 (called mass flux-derived ODP from now on) explains 71% of the variance of the original
281 trajectory-derived ODP fields for the time period 1999-2006. We find good agreement
282 between the trajectory-derived and the mass flux-derived ODP and ODP-weighted CHBr_3
283 emissions (see Sections 4 and 5 for details). In order to extend the ODP-weighted CHBr_3
284 emissions beyond 1999 and 2006, we apply the linear fit function $[a_0, a_1]$ to the convective
285 upward mass flux between 250 and 80 hPa from ERA-Interim and from the CESM1-CAM5
286 runs. Thus we estimate observational (1979-2013), model historical (1979-2005) and model
287 future RCP8.5 (2006-2100) mass flux derived-ODP fields.

288
289 The ODP of such short-lived substances as CHBr_3 shows a weak dependence on the
290 stratospheric residence time and thus on the latitude of the injection point at the tropopause
291 (Pisso et al., 2010). Our method of deriving the ODP from the convective mass flux neglects
292 the impact of spatial variations in the stratospheric residence time on the ODP. However,
293 within the tropical belt, which is the main region of interest for our analysis with high ODP
294 values and strong convective mass fluxes, the stratospheric residence time can be
295 approximated by a constant as included in the fit coefficients. Similarly, expected future
296 changes of the stratospheric residence time associated with an accelerating stratospheric
297 circulation (Butchart, 2014) are not taken into account in our calculation of the mass flux-
298 derived ODP from model climate predictions. ~~While the impact of brominated VSLs on~~
299 ~~stratospheric ozone is expected to change for changing stratospheric residence time, their~~
300 ~~ODP will be less affected. For all gases, the ODP is calculated as a measure of their~~

301 ~~contribution to stratospheric ozone destruction relative to that of CFC-11. Active chlorine~~
302 ~~from CFC-11 will be impacted by changes in the stratospheric circulation in the same way as~~
303 ~~active bromine from CHBr₃, and thus changes in the residence time of the active halogens~~
304 ~~will have no impact on the ODP. On the other hand, changes in the residence time of the long-~~
305 ~~lived halogen source gases such as CFC-11 can change the efficiency of chlorine release and~~
306 ~~thus indirectly impact the ODP of shorter-lived gases. However, the expected impact of~~
307 ~~changing stratospheric chlorine background levels will be orders of magnitude larger than the~~
308 ~~impact of the release efficiency.~~ Overall, we expect that tropospheric transport and
309 stratospheric chemistry will have a much larger impact on the future ODP trends than changes
310 in the stratospheric residence time. Thus, we do not take the latter into account in our
311 calculation of future ODP-weighted CHBr₃ emissions for the benefit of a cost-efficient
312 method enabling the estimation of future ODP fields.

313

314 In addition to changing mass fluxes included in our ODP proxy, changes in stratospheric
315 chemistry will impact the future ODP of CHBr₃. In order to account for less effective catalytic
316 ozone destruction, we apply a changing α -factor to our ODP fields. The bromine α -factor
317 describes the chemical effectiveness of stratospheric bromine ozone depletion relative to
318 chlorine (Daniel et al., 1999) and is set to a global mean value of 60 (Sinnhuber et al., 2009)
319 for the calculation of 1999-2006 ODP fields (Section 2.2). As most of the bromine induced
320 stratospheric ozone loss is caused by the combined BrO/ClO catalytic cycle, the effect of
321 bromine (and thus the α -factor) is expected to be smaller for decreasing anthropogenic
322 chlorine. We use idealized experiments carried out with the UM-UKCA chemistry-climate
323 model to derive changes in the α -factor of brominated VLSLs. The experiments were
324 performed under two different stratospheric chlorine concentrations, corresponding roughly to
325 beginning (3 ppbv Cl_y) and end (0.8 ppbv Cl_y) of the 21st century conditions, and 1xVLSL
326 versus 2xVLSL loading (see Yang et al., 2014 for details). We calculate the difference
327 between the 2xVLSL and 1xVLSL simulations for both chlorine scenarios to get the overall
328 effect of VLSL on ozone for the beginning and end of the 21st century conditions. From the
329 change of this difference from one chlorine scenario to the other, we estimate the global mean
330 α -factor applicable for bromine from VLSL at the end of the century to be around 47.
331 Compared to the current α -factor of 60 this is a reduction of about 22%. For simplicity, we
332 assume the stratospheric chlorine loading from 2000 to 2100 to be roughly linear and estimate
333 the α -factor within this time period based on a linear interpolation between the 2000 and the
334 2100 value. In a similar manner, we scale the ODP field before 1996 to account for the fact

335 that during this time there was less stratospheric chlorine and a reduced effectiveness of
336 bromine-related ozone depletion. Stratospheric chlorine in 1979 equals roughly the value
337 expected for 2060 (Harris and Wuebbles et al., 2014), thus corresponding to a 13% reduced
338 bromine α -factor of 52. ODP values between 1979 and the year 1996, when the amount of
339 stratospheric chlorine reached a peak and started to level off (Carpenter and Reimann et al.,
340 2014), are estimated based on a linear interpolation over this time period.

341

342 **2.4 ODP-weighted CHBr_3 emissions**

343

344 The concept of ODP-weighted emissions combines information on the emission strength and
345 on the relative ozone-destroying capability of a substance. Its application to VSLS has been
346 recently rendered possible by the availability of observation-based VSLS emission maps
347 (Ziska et al., 2013). Here, we calculate the present-day ODP-weighted emissions of CHBr_3 for
348 data available for four months (March, June, September and December) from 1999 to 2006 by
349 multiplying the CHBr_3 emissions with the trajectory-derived ODP at each grid point. The
350 resulting ODP-weighted emission maps are given as a function of time (monthly averages)
351 and location ($1^\circ \times 1^\circ$ grid). Global annual means are calculated by averaging over all grid
352 points and over the four given months.

353

354 In order to extend the time series of ODP-weighted CHBr_3 emissions beyond 1999 and 2006,
355 we derive ODP fields from the ERA-Interim upward mass flux. The method is based on the
356 polynomial fit determined for the available trajectory-derived CHBr_3 ODP fields as described
357 in Section 2.3. Multiplying the mass flux-derived ODP fields with the monthly mean emission
358 fields from Ziska et al. (2013) results in a long term time series (1979-2013) of ODP-
359 weighted CHBr_3 emissions. Similarly, we use the CESM1-CAM5 mass flux-derived ODP
360 fields together with emission inventories derived from CESM1-CAM5 meteorological data to
361 produce historical (1979-2005) and future (2006-2100) model-driven ODP-weighted CHBr_3
362 emission fields.

363

364 **3 ODP-weighted CHBr_3 emissions for present day conditions**

365

366 We will introduce the concept of the ODP-weighted emissions of CHBr_3 exemplarily for
367 March 2005 and discuss how the ODP-weighted emissions of this very short-lived compound
368 compare to those of long-lived halogens. The CHBr_3 emissions (Ziska et al., 2013) for March

369 2005 are shown in Figure 1a with highest emissions in coastal regions, in the upwelling
370 equatorial waters and the Northern Hemisphere (NH) mid-latitude Atlantic. The emissions
371 show large variations and reach values higher than $1500 \text{ pmol m}^{-2} \text{ hr}^{-1}$ in coastal regions
372 characterized by high concentrations due to biological productivity and anthropogenic
373 activities. In the tropical open ocean, emissions are often below $100 \text{ pmol m}^{-2} \text{ hr}^{-1}$, while in
374 the subtropical gyre regions, ocean and atmosphere are nearly in equilibrium and fluxes are
375 around zero. Globally, the coastal and shelf regions account for about 80% of all CHBr_3
376 emissions (Ziska et al., 2013). Apart from the gradients between coastal, shelf and open ocean
377 waters the emissions show no pronounced longitudinal variations. Negative emissions occur
378 in parts of the Southern Ocean, northern Pacific and North Atlantic and indicate a CHBr_3 sink
379 given by a flux from the atmosphere into the ocean. **The evaluation of various CHBr_3
380 emission inventories from Hossaini et al. (2013) shows that in the tropics the best
381 agreement between model and observations is achieved using the bottom-up emissions
382 from Ziska et al. (2013). In the extratropics, however, the CHBr_3 emissions from Ziska
383 are found to result in too low atmospheric model concentrations diverging from
384 observations by 40 to 60%.**

385
386 The potential impact of CHBr_3 on the stratospheric ozone layer is displayed in Figure 1b in
387 form of the ODP of CHBr_3 given as a function of time and location of the emissions but
388 independent of its strength. Overall, the ODP of CHBr_3 is largest in the tropics (tropical ODP
389 belt) and has low values (mostly below 0.1) north and south of 20° . The ODP depends
390 strongly on the efficiency of rapid transport from the ocean surface to the stratosphere which
391 is in turn determined by the intensity of high reaching convection. In the NH winter/spring of
392 most years, the strongest convection and therefore the highest ODP values of up to 0.85 are
393 found over the equatorial West Pacific (Pisso et al., 2010). In contrast to the CHBr_3 emission
394 estimates, the ODP shows pronounced longitudinal variations linked to the distribution of
395 convection and low-level flow patterns.

396
397 The ODP-weighted CHBr_3 emissions for March 2005 are displayed in Figure 2. While the
398 emissions themselves describe the strength of the CHBr_3 sea-to-air flux, the ODP-weighted
399 emissions cannot be interpreted directly as a physical quantity but only relative to ODP-
400 weighted emissions of long-lived halocarbons. The spatial distribution of the ODP-weighted
401 emissions combines information on where large amounts of CHBr_3 are emitted from the
402 ocean and where strong vertical transport enables CHBr_3 to reach the stratosphere. Only for

403 regions where both quantities are large, strong ODP-weighted emissions will be found.
404 Regions where one of the quantities is close to zero will not be important, such as the mid-
405 latitude North Atlantic where large CHBr_3 emissions occur but the ODP is very low. Negative
406 ODP-weighted emissions occur in regions where the flux is from the atmosphere into the
407 ocean. Since negative ODP-weighted emissions are not a meaningful quantity and occur in
408 regions where the ODP is small they will not be displayed in the following figures and are not
409 taken into account for the calculations of the global mean values. The ODP-weighted
410 emissions are in general largest between 20°S and 20°N (72% of the overall global amount)
411 as a result of the tropical ODP belt and peak at the equator and tropical coast lines as a result
412 of the emission distribution. The distribution of the ODP-weighted emissions demonstrates
413 clearly that CHBr_3 emissions from the NH and Southern Hemisphere (SH) extratropics have
414 negligible impact on stratospheric ozone chemistry. **Thus, the fact that the emissions from**
415 **Ziska et al. (2013) might be too low in the extratropics (Hossaini et al., 2013) does not**
416 **impact our results.** Of particular importance for the stratosphere, on the other hand, are
417 emissions from the Maritime Continent (South-East Asia), the tropical Pacific and the Indian
418 Ocean.

419
420 The global annual mean ODP-weighted emissions of CHBr_3 are about 40 Gg/year for 2005
421 (Figure 3) based on the March, June, September and December values of this year. The
422 concept of ODP-weighted emissions becomes particularly useful when comparing this
423 quantity for CHBr_3 with the ones of human-made halocarbons. For the year 2005, ODP-
424 weighted emissions of CHBr_3 amount up to 50% of the ODP-weighted emissions of methyl
425 bromide (CH_3Br , natural and anthropogenic), of CFC-11, or of CFC-12 (CCl_2F_2) and are of
426 similar magnitude as the ODP-weighted emissions of CCl_4 and the individual halons. While
427 the ODP of CHBr_3 exceeds the value of 0.5 only in less than 10% over the globe, the
428 relatively large CHBr_3 emissions make up for the overall relatively small ODPs. Current
429 estimates of global CHBr_3 emissions range between 249 Gg/year and 864 Gg/year (Ziska et
430 al., 2013 and references therein), with the higher global emission estimates coming from top-
431 down methods while the lower boundary is given by the bottom-up study from Ziska et al.
432 (2013). Already this lower boundary of the unweighted CHBr_3 emissions, exceeds the combined
433 emissions of the most abundant CFCs. For our study, even the choice of the lowest emission
434 inventory leads to relatively large ODP-weighted emissions of the very short-lived CHBr_3 as
435 discussed above. Choosing a different emission inventory than Ziska et al. (2013) would
436 result in even larger ODP-weighted CHBr_3 emissions. Still more important than the overall

437 CHBr₃ emission strength is the fact that emissions and ODP show the same latitudinal
438 gradients with both fields having higher values at the low latitudes. This spatial coincidence
439 of large sources and efficient transport causes the relatively large global mean value of ODP-
440 weighted CHBr₃ emissions.

441

442 It is important to keep in mind that the long-lived halocarbons are to a large degree of
443 anthropogenic origin, while CHBr₃ is believed to have mostly natural sources. However,
444 CHBr₃ in coastal regions also results from anthropogenic activities such as aqua-farming in
445 South-East Asia (Leedham et al., 2013) and oxidative water treatment (Quack and Wallace,
446 2003). While these sources accounted for only a small fraction of the global budget in 2003
447 (Quack and Wallace, 2003), their impact is increasing. **In particular, aqua-farming used,
448 among other things, for food production and CO₂ sequestering has started to increase as
449 an anthropogenic VLS source. Leedham et al. (2013) estimated tropical halocarbon
450 production from macroalgae in the Malaysian coastal region and suggest that only 2% of
451 the local CHBr₃ emissions originate from farmed seaweeds. However, based on recent
452 production growth rates, the Malaysian seaweed aquaculture has been projected to
453 experience a 6-11 fold increase over the next years (Phang et al., 2010). More
454 importantly, other countries such as Indonesia, Philippines and China are known to
455 produce considerably more farmed seaweed than Malaysia (e.g., Tang et al., 2011), but
456 their contribution to the total anthropogenic VLS emissions has not yet been assessed.
457 The ODP of CHBr₃ demonstrates the high sensitivity of the South-East Asia region to
458 growing emissions. Globally the highest ODP values (Figure 1b) are found in the same
459 region where we expect future anthropogenic CHBr₃ emissions to increase substantially.
460 An assessment of current and future seaweed farming activities including information
461 on farmed species, fresh or dry weight macro algal biomass and incubation derived
462 halocarbon production values is required to estimate the net oceanic aquaculture VLS
463 production.** Since the general ODP concept has been originally defined for anthropogenic
464 halogens, the ODP-weighted CHBr₃ emissions should be calculated for the anthropogenic
465 component of the emissions. However, since no such estimates are available at the moment,
466 the method is applied to the combined emission field. Given that the natural oceanic
467 production and emissions of halogenated VLS are expected to change in the future due to
468 increasing ocean acidification, changing primary production and ocean surface meteorology
469 (Hepach et al., 2014), it will remain a huge challenge to properly separate natural and
470 anthropogenic emissions of these gases.

471

472

473 **4 ODP proxy**

474

475 It is necessary to understand the short and long-term changes of the ODP-weighted CHBr_3
476 emissions in order to predict their future development. On the seasonal time scales, the ODP-
477 weighted CHBr_3 emissions show large variations as demonstrated in Figure 4 for June and
478 December 2001. In the NH summer, 57% of the ODP-weighted emissions stem from the NH
479 tropical belt (30°N - 0°N) with largest contributions from the Maritime Continent and Asian
480 coastal areas. In the NH winter, the ODP-weighted emissions shift to the SH tropical belt
481 (48%) with strongest contributions from the West Pacific. While the Maritime Continent is an
482 important source region all-year around, emissions from the southern coast line of Asia during
483 NH winter are not very important for stratospheric ozone depletion. The emissions reveal
484 slight seasonal variations (not shown here) due to varying surface wind and sea surface
485 temperature; however, it is the seasonality of the ODP (Figure 5a) that causes the pronounced
486 shift of the ODP-weighted emissions from one hemisphere to the other.

487

488 We want to analyze the long-term changes of ODP-weighted CHBr_3 emissions and thus need
489 to extend the time series beyond 1999 and 2006. While CHBr_3 emissions are available for
490 1979-2013, the ODP itself, based on costly trajectory calculations, is restricted to 1999-2006.
491 In order to develop an ODP proxy, we first analyze the variations of the trajectory-derived
492 ODP fields and their relation to meteorological parameters. The ODP fields for the months
493 June and December 2001 shown in Figure 5a have their maxima between 0°N and 20°N for
494 the NH summer and 5°N and 15°S for the NH winter. In the NH summer, the dominant
495 source region for stratospheric CHBr_3 is located in the equatorial West Pacific region
496 including south-east Asia. In the NH winter, the source region is shifted westward and
497 southward with its center now over the West Pacific. These seasonal variations agree with
498 results from previous trajectory studies (e.g., Fueglistaler et al., 2005; Krüger et al., 2008) and
499 are consistent with the main patterns of tropical convection (Gettelman et al., 2002).

500

501 A detailed picture of the high reaching convective activities for June and December is given
502 in Figure 5b in form of the ERA-Interim monthly mean updraught mass flux between 250 and
503 80 hPa. The rapid updraughts transporting air masses from the boundary layer into the tropical
504 tropopause layer (TTL) are part of the ascending branch of the tropospheric circulation

505 constituted by the position of the intertropical convergence zone (ITCZ). The updraught
506 convective mass fluxes are largest in and near the summer monsoon driven circulations close
507 to the equator. Over the West Pacific and Maritime Continent the region of intense convection
508 is quite broad compared to the other ocean basins due to the large oceanic warm pool and
509 strong monsoon flow. In addition to the overall annual north-south migration pattern, large
510 seasonal changes of the updraught mass flux are visible over South America and the Maritime
511 Continent consistent with the climatological distribution of the ITCZ. The south-east ward
512 pointing extension in the Pacific is strongest in the NH winter and indicates a double ITCZ.

513

514 We derive a CHBr_3 ODP proxy from the ERA-Interim updraught mass fluxes (referred to as
515 mass flux-derived ODP, see Section 2.3 for details). **While the downdraught mass fluxes
516 can also impact (5-15%) the composition in the upper troposphere/lower stratosphere
517 (Frey et al., 2015), they are not included in our proxy since their importance for the
518 contribution of CHBr_3 to stratospheric bromine is less clear and cannot be prescribed
519 by a fit relation.** The strong correlation between CHBr_3 ODP and high-reaching convection
520 justifies our method by indicating that we capture the most important process for explaining
521 the ODP variability. The mass flux-derived ODP fields are shown in Figure 5c and explain
522 76% and 81% of the variance of the original trajectory-derived ODP fields (Figure 5a).
523 Differences between the trajectory-derived ODP fields and the mass flux-derived proxy may
524 be caused by the fact that not only the location of the most active convective region will
525 determine the ODP distribution but also patterns of low-level flow into these regions.
526 Additionally, spatial and seasonal variations in the expected stratospheric residence time may
527 have a small impact on the trajectory-derived ODP and cause deviations to the mass flux-
528 derived proxy. Largest disagreement between the trajectory-derived and mass flux-derived
529 ODP is found over South America and Africa. However, the ODP values over the continents
530 are not important for the ODP-weighted CHBr_3 emissions due to the very low to non-existent
531 emissions over land (Quack and Wallace, 2003) and are not used in our study.

532

533 Our analysis confirms that the ODP of species with short lifetimes, such as CHBr_3 , is to a
534 large degree determined by the high-reaching convective activity (Pisso et al., 2010). As a
535 result, updraught mass flux fields can be used to derive a proxy of the ODP fields. Such a
536 proxy can also be derived from related meteorological parameters such as the ERA-Interim
537 detrainment rates (not shown here). The ODP proxies identified here provide a cost-efficient
538 method to calculate ODP fields for past (ERA-Interim) and future (climate model output)

539 meteorological conditions. Long-term changes in stratospheric chemistry due to declining
540 chlorine background levels are taken into account by variations of the bromine α -factor (see
541 Section 2.3 for details). Our method enables us to analyze long-term changes of the ODP and
542 the ODP-weighted emissions, which would otherwise require very large computational
543 efforts.

544

545 **5 ODP-weighted CHBr_3 emissions for 1979-2013**

546

547 Based on the ODP proxy and the correction of the α -factor introduced in Section 4, we
548 calculate ODP-weighted CHBr_3 emission fields for the ERA-Interim time period from 1979 to
549 2013. As a test for our method, we compare the global mean ODP-weighted emissions based
550 on the trajectory- and mass flux-derived ODP fields for the years 1999-2006. The two time
551 series of ODP-weighted emissions are displayed in Figure 6 and show a very good agreement
552 with slightly lower mass flux-derived values (green line) than trajectory-derived values (black
553 line). Individual months can show stronger deviations, e.g., for December 1999 the mass flux-
554 derived ODP-weighted emissions are about 30% smaller than the trajectory-derived ones. The
555 pronounced seasonal cycle with maximum values in the NH summer and autumn is captured
556 by both methods. The seasonal cycle of the global mean values is mostly caused by the very-
557 high ODP-weighted emissions along the South-East Asian coast line which are present during
558 the NH summer/autumn, but not during the NH winter. Note that the ODP-weighted
559 emissions of long-lived halocarbons discussed in Section 3 show no strong seasonal
560 variations. The good agreement between the trajectory-derived and the mass flux-derived
561 ODP-weighted CHBr_3 emissions encourages the use of the latter for the analysis of longer
562 time series.

563

564 The 35-year long time series (1979-2013) of ODP-weighted CHBr_3 emissions is based on the
565 ERA-Interim surface parameters, TTL convective mass flux and a changing bromine α -factor
566 (Figure 7a). The time series is relatively flat over the first 27 years ranging from 34 Gg/year
567 to 39 Gg/year. Over the last years from 2006 to 2013, a steep increase occurred and ODP-
568 weighted CHBr_3 emissions of more than 41 Gg/year are reached. In order to analyze which
569 component, the mass flux-derived ODP fields, the oceanic emissions or the stratospheric
570 chemistry, causes this steep increase, three sensitivity studies are performed. In the first study,
571 the emissions vary over the whole time period (1979-2013), while the ODP field and the
572 bromine α -factor are held fixed at their 35-year mean values. Changes in the resulting, global

573 mean ODP-weighted emission time series (Figure 7b) are driven by changes in the emissions
574 alone and show a steady increase over the whole time period of about 2.2% per decade. This
575 is in agreement with the linear trend of the global mean CHBr_3 emissions estimated to be
576 7.9% over the whole time period caused by increasing surface winds and sea surface
577 temperatures (Ziska et al., in prep). We do not necessarily expect the two trends to be
578 identical, since the ODP-weighted emissions only include emissions in convective active
579 regions, while the global mean emissions correspond to non-weighted mean values including
580 CHBr_3 emissions from middle and high latitudes.

581

582 For the second study, the emission fields and the α -factor are kept constant at the 35-year
583 mean values and the mass flux-derived ODP is allowed to vary with time. Changes in the
584 resulting, global mean ODP-weighted emission time series (Figure 7c) are mainly driven by
585 changes in the tropical high-reaching convection and show a negative trend from 1979 to
586 2005 of -3.4% per decade. Over the years 2006-2013, however, changes in convective activity
587 lead to a steep increase of the ODP-weighted emissions. These changes can either result from
588 a general strengthening of the tropical convective activity or from changing patterns of
589 convective activity, shifting regions of high activity so that they coincide with regions of
590 strong CHBr_3 emissions. For the third sensitivity study, the emissions and mass flux-derived
591 ODP are kept constant at the 35-year mean values, while the α -factor varies with time
592 according to the stratospheric chlorine loading. ODP-weighted CHBr_3 emissions increase by
593 13% from 1979 to 1999 and peak during the time of the highest stratospheric chlorine loading
594 from 1999 to 2006. Overall, variations of the ODP-weighted CHBr_3 emissions induced by the
595 stratospheric chlorine-related chemistry are in the same range as the variations induced by
596 changes in convective transport and oceanic emissions.

597

598 Combining the conclusions of all three sensitivity studies reveals that for the time period 1979
599 to 2005, the positive trend of the emissions and the α -factor on the one hand and the negative
600 trend of the mass flux-derived ODP on the other hand mostly cancel out leading to a flat time
601 series of ODP-weighted CHBr_3 emissions (Figure 7a) with no long-term changes. From 2005
602 to 2013, however, a strong increase in ODP and continuously increasing emissions lead to a
603 step-like increase of the ODP-weighted CHBr_3 emissions from 35 Gg/year to 41 Gg/year.

604

605 **6 Model-derived ODP-weighted CHBr_3 emissions**

606

607 We aim to estimate ODP-weighted CHBr_3 emissions from earth system model runs.
608 Therefore, we use CHBr_3 emissions and the CHBr_3 ODP proxy calculated with CESM1-
609 CAM5 sea surface temperature, surface wind and upward mass flux, respectively (see Section
610 2 for details). In a first step, we evaluate how well the results of our analysis based on the
611 earth system model compare to the results based on ERA-Interim. Figure 8a shows the
612 distribution of the three quantities, CHBr_3 emissions, mass flux-derived ODP and ODP-
613 weighted emissions, for ERA-Interim and CESM1-CAM5 exemplary for March 2000. The
614 distribution of the emission field is very similar between ERA-Interim and CESM1-CAM5.
615 Largest deviations are found in the Indian Ocean along the equator, where higher surface
616 winds and temperatures in the model force a stronger sea-to-air flux. Note that in this region,
617 very limited observational data was available for the construction of the emission inventories
618 and future updates will reveal, if these isolated data points are representative for the equatorial
619 Indian Ocean.

620

621 The ERA-Interim mass flux-derived CHBr_3 ODP (Figure 8b) shows an almost zonally
622 uniform region of higher ODP values (around 0.4) extending south of the equator down to
623 20°S . In contrast, the CESM1-CAM5 mass flux-derived ODP shows only three regions in the
624 inner tropics (the Maritime continent, Africa, South America) with values exceeding 0.3.
625 While the ODP from CESM1-CAM5 can reach locally higher values than the ODP from
626 ERA-Interim, the globally averaged ODP field is larger for the reanalysis data than for the
627 model. As a result, the ODP-weighted CHBr_3 emissions (Figure 8c) based on reanalysis data
628 are higher in most of the tropics. Particularly, in the East Pacific and Indian Ocean large scale
629 features of enhanced ODP-weighted CHBr_3 emissions exist for ERA-Interim but not for the
630 earth system model. On the other hand, enhanced ODP-weighted emissions along some coast
631 lines are present in the model results (e.g., Indonesia) but are not as pronounced in ERA-
632 Interim. Overall, the ODP-weighted CHBr_3 emissions for March 2000 based on ERA-Interim
633 and CESM1-CAM5 show a similar distribution and similar magnitude. The model-derived
634 values are slightly smaller than the observation-derived values mostly as a result of less high-
635 reaching convective activity in the model.

636

637 We compare the global mean ODP-weighted CHBr_3 emissions based on the ERA-Interim
638 reanalysis data (observation-derived) to the same quantity from the CESM1-CAM5 historical
639 model run for the 1999-2006 time period (Figure 9). The historical ODP-weighted emissions
640 from CESM1-CAM5 show larger variations than the observation-derived time series. The

641 stronger variability is caused by a stronger variability in the ODP time series possibly related
642 to larger meteorological fluctuations in the earth system model during this short time period.
643 The overall magnitude as well as the phase and amplitude of the seasonal cycle are reasonably
644 well captured by CESM1-CAM5, encouraging the use of the model to estimate ODP-
645 weighted CHBr_3 emissions for future climate scenarios. Recent improvements have been
646 reported in the regional cloud representation in the deep convective tropical Pacific (Kay et
647 al., 2012) and in the parameterization of deep convection and ENSO simulation (Neale et al.,
648 2008). Overall, our analysis demonstrates that the spatial and seasonal variability of the model
649 fields allows to derive realistic ODP-weighted CHBr_3 emission estimates.

650

651 **7 ODP-weighted CHBr_3 emissions for 2006-2100**

652

653 Future ODP-weighted CHBr_3 emissions shown in Figure 10a are based on future model
654 estimates of the CHBr_3 emissions and the CHBr_3 ODP proxy. Both quantities are calculated
655 based on the meteorological and marine surface variables and convective mass flux from the
656 CESM1-CAM5, RCP8.5 runs. In addition, we have applied a correction factor to the ODP
657 fields to account for a changing α -factor based on less effective ozone loss cycles in the
658 stratosphere due to the decrease of anthropogenic chlorine (Section 2.3). The future estimates
659 of the ODP-weighted CHBr_3 emissions show pronounced interannual variations of up to 20%.
660 Overall, the ODP-weighted emissions increase steadily until 2100 by about 31% of the 2006-
661 2015 mean value corresponding to a linear trend of 2.6% per decade.

662

663 In order to analyze what causes the strong interannual variability and the long-term trend, we
664 conduct sensitivity studies where only one factor (emissions, mass flux-derived ODP,
665 stratospheric chemistry) is changing while the other two are kept constant. Figure 10b
666 displays the time series of ODP-weighted CHBr_3 emissions for varying oceanic emission
667 fields. The emission-driven time series for 2006-2100 shows a positive trend of 2.2% per
668 decade which is in the range of the trend observed for the emission-driven time series for
669 1979-2013 based on ERA-Interim (Figure 7b). However, the model-based ODP-weighted
670 emissions show no long-term change over the first 15 years and the positive, emission-driven
671 trend only starts after 2020. The second sensitivity study (Figure 10c) highlights changes in
672 the ODP-weighted emissions attributable to high-reaching convection (via the mass flux-
673 derived ODP), while emission fields and α -factor are kept constant. Clearly, the strong
674 interannual variations in the combined time series (Figure 10a) are caused by the same

675 fluctuations in the mass flux-driven time series. In comparison, the interannual variability of
676 the emission-driven time series is less pronounced. The projected changes in atmospheric
677 transport cause a positive trend of the ODP-weighted emissions of about 3.1% per decade.
678 This positive trend projection in the mass flux-derived ODP reveals a future change in the
679 tropical circulation with significant consequences for trace gas transport from the troposphere
680 into the stratosphere. **More detailed evaluations demonstrate that the CESM1-CAM5
681 tropical convective upward mass flux is projected to decrease in the lower and middle
682 troposphere (not shown here) in agreement with results from UKCA chemistry-climate
683 model simulations (Hossaini et al., 2012). Contrary to the changes in the middle
684 troposphere, the convective mass flux in the upper troposphere (above the 250 hPa
685 level), is projected to increase in the future again in agreement with Hossaini et al.
686 (2012). A higher extension of tropical deep convection has also been found in other
687 model projections and global warming leading to an uplift of the tropopause has been
688 suggested as the possible cause (Chou and Chen, 2010; Rybka and Tost, 2014). Overall,
689 an increasing upward mass flux in the upper troposphere/lower stratosphere would lead
690 to enhanced entrainment of CHBr_3 into the stratosphere, consistent with results from
691 Hossaini et al. (2012) and Dessens et al. (2009), and thus to increasing ODP-weighted
692 emissions.** Finally, for the last sensitivity study, the chemistry-driven time series of the ODP-
693 weighted emissions shows no interannual variability and a negative trend of -2.6% per
694 decade. Decreasing anthropogenic chlorine emissions and thus a less efficient BrO/ClO ozone
695 loss cycle lead to a reduction of bromine-related ozone depletion of 22% as prescribed by the
696 results of the idealized chemistry-climate model experiments from Yang et al. (2014).

697

698 In summary, changing emissions and changing convection lead to a projected increase of the
699 ODP-weighted emissions over the 21st century. If only these two factors would impact the
700 ODP-weighted emissions, a positive trend of 5.4% per decade would be expected based on
701 RCP8.5 model simulations. However, due to declining anthropogenic chlorine, stratospheric
702 ozone chemistry will become less effective and the corresponding decreasing α -factor reduces
703 the ODP-weighted CHBr_3 emissions resulting in an overall projected trend of about 2.6% per
704 decade.

705

706 A comparison of the model-derived CHBr_3 ODP-weighted emissions with the ones of other
707 long-lived substances is shown in Figure 11. For the other ozone depleting substances
708 included in the comparison, changing emissions are taken into account by applying their

709 potential emission scenarios (Velders et al., 2007; Ravishankara et al., 2009). The ODP of
710 CFC-11 is nearly independent of the stratospheric chlorine levels (Ravishankara et al.,
711 2009), and is thus kept constant for the whole time period. The same is assumed for all other
712 long-lived halocarbons included in the comparison. Our comparison shows that emissions of
713 the short-lived CHBr_3 can be expected to have a larger impact on stratospheric ozone than the
714 other anthropogenic halocarbons after approximately 2025 (Figure 11). Two exceptions to
715 this are ODP-weighted emissions of CH_3Br and anthropogenic N_2O (Ravishankara et al.,
716 2009) both not shown in our plot.

717
718 CH_3Br , with partially anthropogenic and partially natural sources, is not included in the
719 comparison, since no potential emission scenario and no estimate on how changes in
720 atmospheric transport will impact its ODP are available at the moment. If we would assume a
721 CH_3Br scenario with constant emissions from natural and anthropogenic sources and a
722 constant α -factor, its ODP weighted emissions would be around 70 Gg/year over the 21st
723 century. However, we know this to be unrealistic and expect changes in anthropogenic CH_3Br
724 emissions and a decreasing α -factor which would both lead to smaller projections of its ODP-
725 weighted emissions. N_2O emissions have been projected to be the most important ozone-
726 depleting emissions in the future with ODP-weighted emissions between 100 and 300 Gg/year
727 expected for the end of the century (Ravishankara et al., 2009).

728

729 **8 Discussion and summary**

730

731 The ODP-weighted emissions of CHBr_3 give a detailed picture on where and when oceanic
732 CHBr_3 emissions take place that will later impact stratospheric ozone. Furthermore, they
733 provide a useful tool of comparing the emission strength of CHBr_3 with the ones of long-lived
734 anthropogenic gases in an ozone depletion framework. Since currently no information is
735 available on the strength of anthropogenic CHBr_3 emissions, the ODP concept is applied to
736 the complete emission budget including the natural oceanic contribution. While we focus our
737 analysis on one VSLs and introduce the method and application **within a case-study**
738 **framework** for CHBr_3 , the concept can be applied to all VSLs where emissions and ODP are
739 available at a spatial resolution necessary to describe their variability.

740

741 While the ODP-weighted emissions are an important step towards assessing the current and
742 future effects of VSLs on the ozone layer, one needs to keep in mind that the absolute values

743 are subject of large uncertainties arising from uncertainties in the emission inventories and in
744 the parameterization of the convective transport. **Existing global CHBr₃ emission**
745 **inventories show large discrepancies due to sparse observational data sets and a**
746 **particular high uncertainty in coastal emissions from differing types and amounts of**
747 **macroalgae (Carpenter and Reimann et al., 2014). We have used the Ziska et al. (2013)**
748 **emission inventory which suggests a lower flux of CHBr₃ from the tropical oceans to the**
749 **atmosphere than the other inventories. Based on comparison of the emission inventories**
750 **in Hossaini et al. (2013) we would expect that the application of a different emission**
751 **scenario in our approach could lead to two to three times higher ODP-weighted**
752 **emissions. However, for the tropics, the relatively low emissions from Ziska et al. (2013)**
753 **provide the best fit with the limited available atmospheric data (Hossaini et al., 2013).**

754 The sensitivity of our results to uncertainties in transport becomes apparent when we apply
755 the ODP fields calculated from FLEXPART trajectories without taking into account
756 convective parameterization (Pisso et al., 2010). The ODP calculated without convective
757 parameterization results in roughly 50% lower global mean ODP-weighted CHBr₃ emissions.
758 Additionally, uncertainties may arise from the simplified tropospheric and stratospheric
759 chemistry schemes with an altitude-independent α -factor and a prescribed tropospheric
760 lifetime. Further detailed studies including different convective parameterization schemes,
761 more detailed representation of tropospheric chemistry, product gas impacts, various emission
762 inventories and multi-model mean scenarios are required in order to obtain reliable
763 uncertainty ranges which need to be included in any communication of ODPs to policy
764 makers.

765
766 Our analysis reveals that the spatial variability of trajectory-derived ODP fields of species
767 with short lifetimes, such as CHBr₃, is to a large degree determined by deep tropical
768 convection. As a result, a cost-efficient method to calculate ODP field proxies from updraught
769 mass flux fields has been developed and applied. Past ODP-weighted CHBr₃ emission
770 estimates have been derived based on ERA-Interim meteorological fields. For the time period
771 1979 to 2005, a positive trend in the CHBr₃ emissions and a negative trend in mass flux-
772 derived ODP mostly cancel out leading to a flat time series of ODP-weighted emissions with
773 no long-term changes. From 2006 to 2013, however, a strong increase in both quantities leads
774 to a step-like increase of the ODP-weighted CHBr₃ emissions.

775

776 Future ODP-weighted CHBr_3 emission estimates have been derived from CESM1-CAM5
777 RCP8.5 runs taking into account changing meteorological and marine surface parameters,
778 convective activity and stratospheric chemistry. Changes in tropospheric chemistry and
779 stratospheric residence time are not taken into account for the calculation of the future ODP-
780 weighted emissions. While our methodology is somewhat limited by these simplifications,
781 CHBr_3 delivery from the surface to the tropopause in a future changing climate is expected to
782 be mostly related to changes in tropospheric transport rather than changes in tropospheric
783 chemistry (Hossaini et al., 2013) suggesting that we include the most important processes
784 here. Furthermore, we do not account for changing biogeochemistry in the ocean and
785 anthropogenic activities that can lead to increasing CHBr_3 emissions and further amplify the
786 importance of VSLS for stratospheric ozone chemistry. Such changes in the oceanic sources
787 are important for estimating the future impact of VSLS on atmospheric processes, but are not
788 understood well enough yet to derive reliable future projections. **Finally, we do not consider**
789 **potential future changes in stratospheric aerosol which could impact the contribution of**
790 **VSLS to stratospheric ozone depletion (Salawitch et al., 2005; Sinnhuber et al., 2006).**
791 **Variations in the background stratospheric aerosol loading (e.g., Vernier et al., 2011)**
792 **are mostly attributed to minor volcanic eruptions (Neely et al., 2013). Since future**
793 **volcanic eruptions are not accounted for in the simulations scenarios used here, we do**
794 **not include the impact of natural aerosol variations. Suggested future geo-engineering**
795 **would intentionally enhance the stratospheric aerosol loading and is projected to**
796 **increase the impact of VSLS on stratospheric ozone by as much as 2% at high latitudes**
797 **(Tilmes et al., 2012). Such a scenario is not included in our simulations, but could**
798 **effectively enhance the ODP of CHBr_3 due to an enhanced BrO/ClO ozone loss cycle in**
799 **the lower stratosphere (Tilmes et al., 2012).** Overall, some discrepancies between the
800 observation- and model-derived ODP-weighted CHBr_3 emissions exist, very likely related to
801 out of phase tropical meteorology in the model. However, there is general good agreement
802 between the spatial and seasonal variability of the observation- and model-derived fields,
803 giving us confidence to use this model to derive realistic ODP-weighted CHBr_3 emission
804 estimates.

805

806 Variability of the ODP-weighted CHBr_3 emissions on different time scales are driven by
807 different processes. Spatial and seasonal variations are caused by variations in the surface to
808 tropopause transport via deep convection. Inter-annual variability is mostly driven by
809 transport but also by the variability in the oceanic emissions. Both processes are weakly

810 correlated on inter-annual time scales (with a Pearson correlation coefficient between the
811 interannual anomalies of $r=0.3$), suggesting that in years with stronger emissions (driven by
812 stronger surface winds and higher temperatures) stronger troposphere-stratosphere transport
813 exist. The long-term trend, finally, can be attributed in equal parts to changes in emissions,
814 tropospheric transport and stratospheric chemistry. While growing oceanic emissions and
815 changing convective activity lead to increasing ODP-weighted CHBr_3 emissions, the expected
816 decline in stratospheric chlorine background levels has the opposite effect and leads to a
817 decrease. Taking all three processes into account, the future model projections suggest a 31%
818 increase of the ODP-weighted CHBr_3 emissions until 2100 for the RCP8.5 scenario. This
819 anthropogenically driven increase will further enhance the importance of CHBr_3 for
820 stratospheric ozone chemistry.

821

822 **Acknowledgements** The authors are grateful to the ECMWF for making the reanalysis
823 product ERA-Interim available. This study was carried out within the EU project SHIVA
824 (FP7-ENV-2007-1-226224) and the BMBF project ROMIC THREAT (01LG1217A). We
825 thank Steve Montzka for helpful discussions.

826 **References**

827

828 Aschmann, J. and Sinnhuber, B.-M.: Contribution of very short-lived substances to
829 stratospheric bromine loading: uncertainties and constraints, *Atmos. Chem. Phys.*, 13, 1203-
830 1219, doi:10.5194/acp-13-1203-2013, 2013.

831

832 Austin, J., N., and Butchart, N.: Coupled chemistry-climate model simulations for the period
833 1980 to 2020: ozone depletion and the start of ozone recovery, *Quarterly Journal of the Royal*
834 *Meteorological Society*, 129: 3225–3249, 2006.

835

836 Braesicke, P., Keeble, J., Yang, X., Stiller, G., Kellmann, S., Abraham, N. L., Archibald, A.,
837 Telford, P., and Pyle, J. A.: Circulation anomalies in the Southern Hemisphere and ozone
838 changes, *Atmos. Chem. Phys.*, 13, 10677– 10688, doi:10.5194/acp-13-10677-2013, 2013.

839

840 Brioude, J., R. W. Portmann, J. S. Daniel, O. R. Cooper, G. J. Frost, K. H. Rosenlof, C.
841 Granier, A. R. Ravishankara, S. A. Montzka, and A. Stohl: Variations in ozone depletion
842 potentials of very short-lived substances with season and emission region. *Geophys. Res.*
843 *Lett.*, 37, L19804, doi:10.1029/2010GL044856, 2010.

844

845 Butchart, N.: The Brewer-Dobson circulation, *Rev. Geophys.*, 52,
846 doi:10.1002/2013RG000448, 2014.

847

848 L.J. Carpenter and S. Reimann (Lead Authors), J.B. Burkholder, C. Clerbaux, B.D. Hall, R.
849 Hossaini, J.C. Laube, and S.A. Yvon-Lewis, Ozone-Depleting Substances (ODSs) and Other
850 Gases of Interest to the Montreal Protocol, Chapter 1 in *Scientific Assessment of Ozone*
851 *Depletion: 2014*, Global Ozone Research and Monitoring Project–Report No. 55, World
852 Meteorological Organization, Geneva, Switzerland, 2014.

853

854 **Chou, C. and Chen, C.: Depth of Convection and the Weakening of Tropical Circulation**
855 **in Global Warming. *J. Climate*, 23, 3019–3030, doi: doi:10.1175/2010JCLI3383.1, 2010.**

856

857 Daniel, J. S., Solomon, S., Portmann, R. W., and Garcia, R. R.: Stratospheric ozone
858 destruction: The importance of bromine relative to chlorine, *J. Geophys. Res.*, 104, 23871–
859 23880, 1999.

860

861 Dee, D. P., et al.: The ERA-Interim reanalysis: configuration and performance of the data
862 assimilation system, *Quarterly Journal of the Royal Meteorological Society*, 137(656), 553–
863 597, doi:10.1002/qj.828, 2011.

864

865 **Dessens, O., Zeng, G., Warwick, N. and Pyle, J.: Short-lived bromine compounds in the**
866 **lower stratosphere; impact of climate change on ozone, *Atmos. Sci. Lett.*, 10(3), 201–206,**
867 **2009.**

868

869 Dorf, M., J.H. Butler, A. Butz, C. Camy-Peyret, M.P. Chipperfield, L. Kritten, S.A. Montzka,
870 B. Simmes, F. Weidner, and K. Pfeilsticker: Long-term observations of stratospheric bromine
871 reveal slow down in growth, *Geophys. Res. Lett.*, 33, L24803, doi: 10.1029/2006GL027714,
872 2006.

873

874 **Frey, W., R. Schofield, P. Hoor, D. Kunkel, F. Ravagnani, A. Ulanovsky, S. Viciani, F.**
875 **D’Amato, and T. P. Lane, The impact of overshooting deep convection on local**
876 **transport and mixing in the tropical upper troposphere/lower stratosphere (UTLS),**
877 ***Atmospheric Chemistry and Physics*, 15(11), 6467–6486, doi:10.5194/acp-15-6467-2015,**
878 **2015.**

879

880 Fueglistaler, S., M. Bonazzola, P. H. Haynes, and T. Peter: Stratospheric water vapor
881 predicted from the Lagrangian temperature history of air entering the stratosphere in the
882 tropics, *J. Geophys. Res.*, 110, D08107, doi:10.1029/2004JD005516, 2005.

883

884 Gettelman, A., M. L. Salby, and F. Sassi, Distribution and influence of convection in the
885 tropical tropopause region, *J. Geophys. Res.*, 107(D10), doi:10.1029/2001JD001048, 2002.

886

887 N. R. P. Harris and D. J. Wuebbles (Lead Authors), J.S. Daniel, J. Hu, L.J.M. Kuijpers, K.S.
888 Law, M. J. Prather, R. Schofield, Scenarios and Information for Policymakers, Chapter 5 in
889 Scientific Assessment of Ozone Depletion: 2014, Global Ozone Research and Monitoring
890 Project–Report No. 55, World Meteorological Organization, Geneva, Switzerland, 2014.

891

892 Hepach, H., Quack, B., Ziska, F., Fuhlbrügge, S., Atlas, E. L., Krüger, K., Peeken, I., and
893 Wallace, D. W. R.: Drivers of diel and regional variations of halocarbon emissions from the

894 tropical North East Atlantic, *Atmos. Chem. Phys.*, 14, 1255-1275, doi:10.5194/acp-14-1255-
895 2014, 2014.

896

897 Hossaini, R., M. P. Chipperfield, S. Dhomse, C. Ordóñez, A. Saiz-Lopez, N. L. Abraham, A.
898 Archibald, P. Braesicke, P. Telford, and N. Warwick: Modelling future changes to the
899 stratospheric source gas injection of biogenic bromocarbons, *Geophys. Res. Lett.*, 39,
900 L20813, doi:10.1029/2012GL053401, 2012.

901

902 Hossaini, R., Mantle, H., Chipperfield, M. P., Montzka, S. A., Hamer, P., Ziska, F., Quack,
903 B., Krüger, K., Tegtmeier, S., Atlas, E., Sala, S., Engel, A., Bönisch, H., Keber, T., Oram, D.,
904 Mills, G., Ordóñez, C., Saiz-Lopez, A., Warwick, N., Liang, Q., Feng, W., Moore, F., Miller,
905 B. R., Marécal, V., Richards, N. A. D., Dorf, M., and Pfeilsticker, K.: Evaluating global
906 emission inventories of biogenic bromocarbons, *Atmos. Chem. Phys.*, 13, 11819-11838,
907 doi:10.5194/acp-13-11819-2013, 2013.

908

909 **Hossaini, R., M. P. Chipperfield, S. A. Montzka, A. Rap, S. Dhomse, and W. Feng:**
910 **Efficiency of short-lived halogens at influencing climate through depletion of**
911 **stratospheric ozone, *Nature Geosci*, 8(3), 186–190, doi:10.1038/ngeo2363, 2015.**

912

913 Leedham, E. C., C. Hughes, F. S. L. Keng, S.-M. Phang, G. Malin, and W. T. Sturges:
914 Emission of atmospherically significant halocarbons by naturally occurring and farmed
915 tropical macroalgae, *Biogeosciences*, 10, 3615–3633, doi:10.5194/bg-10-3615-2013, 2013.

916

917 Kay, J. E., et al.: Exposing global cloud biases in the Community Atmosphere Model (CAM)
918 using satellite observations and their corresponding instrument simulators, *J. Climate*, 25,
919 5190–5207, 2012.

920

921 Krüger, K., Tegtmeier, S., and Rex, M.: Long-term climatology of air mass transport through
922 the Tropical Tropopause Layer (TTL) during NH winter, *Atmos. Chem. Phys.*, 8, 813-823,
923 doi:10.5194/acp-8-813-2008, 2008.

924

925 Liang, Q., Stolarski, R. S., Kawa, S. R., Nielsen, J. E., Douglass, A. R., Rodriguez, J. M.,
926 Blake, D. R., Atlas, E. L., and Ott, L. E.: Finding the missing stratospheric Br_y: a global

927 modeling study of CHBr_3 and CH_2Br_2 , *Atmos. Chem. Phys.*, 10, 2269-2286, doi:10.5194/acp-
928 10-2269-2010, 2010.

929

930 Liang, Q., Atlas, E., Blake, D., Dorf, M., Pfeilsticker, K., and Schauffler, S.: Convective
931 transport of very short lived bromocarbons to the stratosphere, *Atmos. Chem. Phys.*, 14, 5781-
932 5792, doi:10.5194/acp-14-5781-2014, 2014.

933

934 Montzka, S., et al.: Ozone-depleting substances (ODSs) and related chemicals, in *Scientific*
935 *Assessment of Ozone Depletion: 2010*, Rep. 52, chap. 1, pp. 1–112, Global Ozone Res. and
936 *Monit. Proj.*, World Meteorol. Organ., Geneva, Switzerland, 2011.

937

938 Neale, R. B., J. H. Richter, and M. Jochum: The impact of convection on ENSO: From a
939 delayed oscillator to a series of events. *J. Climate*, 21, 5904–5924, 2008.

940

941 Neale, R. B., and Coauthors: Description of the NCAR Community Atmosphere Model
942 (CAM5.0). NCAR Tech. Rep. NCAR/TN-486+STR, 268 pp, 2010.

943

944 **Neely, R. R., Toon, O. B., Solomon, S., Vernier, J. P., Alvarez, C., English, J. M.,**
945 **Rosenlof, K. H., Mills, M. J., Bardeen, C. G., Daniel, J. S. and Thayer, J. P.: Recent**
946 **anthropogenic increases in SO_2 from Asia have minimal impact on stratospheric aerosol,**
947 ***Geophys. Res. Lett.*, 40(5), 999–1004, doi:10.1002/grl.50263, 2013.**

948

949 Nightingale, P. D., Malin, G., Law, C. S., Watson, A. J., Liss, P. S., Liddicoat, M. I., Boutin,
950 J. and Upstill-Goddard, R. C.: In situ evaluation of air-sea gas exchange parameterizations
951 using novel conservative and volatile tracers, *Global Biogeochemical Cycles*, 14(1), 373–387,
952 doi:10.1029/1999GB900091, 2000.

953

954 **Phang, S.-M., Yeong, H.-Y., Lim, P.-E., Nor, A. R., and Gan, K. T.: Commercial**
955 **varieties of *Kappaphycus* and *Eucheuma* in Malaysia, *Malaysian J. Sci.*, 29, 214–224,**
956 **2010.**

957

958 Pisso, I., Haynes, P. H., and Law, K. S.: Emission location dependent ozone depletion
959 potentials for very short-lived halogenated species, *Atmos. Chem. Phys.*, 10, 12025-12036,
960 doi:10.5194/acp-10-12025-2010, 2010.

961
962 Pyle, J. A., N. Warwick, X. Yang, P. J. Young, and G. Zeng: Climate/chemistry feedbacks
963 and biogenic emissions, *Philos. Trans. R. Soc. A*, 365(1856), 1727–1740,
964 doi:10.1098/rsta.2007.2041, 2007.

965
966 Quack, B., E. Atlas, G. Petrick, and D. W. R. Wallace: Bromoform and dibromomethane
967 above the Mauritanian upwelling: Atmospheric distributions and oceanic emissions, *J.*
968 *Geophys. Res.*, 112(D9), D09312, doi:10.1029/2006JD007614, 2007.

969
970 Ravishankara, A.R., J. S. Daniel, R. W. Portmann: Nitrous oxide (N₂O): The dominant ozone-
971 depleting substance emitted in the 21st century. *Science* 326:123–125, 2009.

972
973 **Rybka, H., and H. Tost: Uncertainties in future climate predictions due to convection**
974 **parameterizations, *Atmospheric Chemistry and Physics*, 14(11), 5561–5576,**
975 **doi:10.5194/acp-14-5561-2014, 2014.**

976
977 Sala, S., Bönisch, H., Keber, T., Oram, D. E., Mills, G., and Engel, A.: Deriving an
978 atmospheric budget of total organic bromine using airborne in situ measurements from the
979 western Pacific area during SHIVA, *Atmos. Chem. Phys.*, 14, 6903-6923, doi:10.5194/acp-
980 14-6903-2014, 2014.

981
982 **Salawitch, R. J., Weisenstein, D. K., Kovalenko, L. J., Sioris, C. E., Wennberg, P. O.,**
983 **Chance, K., Ko, M. K. W., and McLinden, C. A.: Sensitivity of ozone to bromine in the**
984 **lower stratosphere, *Geophys. Res. Lett.*, 32, L05811, doi:10.1029/2004GL021504, 2005.**

985
986 **Schofield, R., S. Fueglistaler, I. Wohltmann, and M. Rex: Sensitivity of stratospheric**
987 **Bry to uncertainties in very short lived substance emissions and atmospheric transport,**
988 ***Atmos Chem Phys*, 11(4), 1379–1392, doi:10.5194/acp-11-1379-2011, 2011.**

989
990 Sinnhuber, B.-M., Sheode, N., Sinnhuber, M., Chipperfield, M. P., and Feng, W.: The
991 contribution of anthropogenic bromine emissions to past stratospheric ozone trends: a
992 modelling study, *Atmos. Chem. Phys.*, 9, 2863-2871, doi:10.5194/acp-9-2863-2009, 2009.

993

994 Sioris, C. E., et al.: Latitudinal and vertical distribution of bromine monoxide in the lower
995 stratosphere from Scanning Imaging Absorption Spectrometer for Atmospheric Chartography
996 limb scattering measurements, *J. Geophys. Res.*, 111, D14301, doi: 10.1029/2005JD006479,
997 2006.

998

999 Solomon, S., M. Mills, L. E. Heidt, W. H. Pollock, and A. F. Tuck: On the evaluation of
1000 ozone depletion potentials, *J. Geophys. Res.*, 97, 825–842, 1992.

1001

1002 **Tang, Q., Zhang, J., and Fang, J.: Shellfish and seaweed mariculture increase**
1003 **atmospheric CO₂ absorption by coastal ecosystems, *Mar. Ecol.-Prog. Ser.*, 424, 97–104,**
1004 **2011.**

1005

1006 Taylor, K. E., R. J. Stouffer, and G. A. Meehl: The CMIP5 experiment design. *Bull. Amer.*
1007 *Meteor. Soc.*, **93**, 485–498, 2012.

1008

1009 Tegtmeier, S., Krüger, K., Quack, B., Atlas, E. L., Pisso, I., Stohl, A. and Yang, X.: Emission
1010 and transport of bromocarbons: from the West Pacific ocean into the stratosphere,
1011 *Atmospheric Chemistry and Physics*, 12(22), 10633–10648, doi:10.5194/acp-12-10633-2012,
1012 2012.

1013

1014 **Tilmes, S., D. E. Kinnison, R. R. Garcia, R. Salawitch, T. Canty, J. Lee-Taylor, S.**
1015 **Madronich, and K. Chance (2012), Impact of very short-lived halogens on stratospheric**
1016 **ozone abundance and UV radiation in a geo-engineered atmosphere, *Atmospheric***
1017 ***Chemistry and Physics*, 12(22), 10945–10955.**

1018

1019 Velders, G. J. M., S. O. Andersen, J. S. Daniel, D. W. Fahey and M. McFarland: The
1020 Importance of the Montreal Protocol in Protecting Climate, *PNAS*, 104:4814 – 4819, doi:
1021 10.1073/pnas.0610328104, 2007.

1022

1023 Vernier, J.-P., et al., Major influence of tropical volcanic eruptions on the stratospheric
1024 aerosol layer during the last decade, *Geophys. Res. Lett.*, 38, L12807,
1025 doi:10.1029/2011GL047563, 2011.

1026 Warwick, N. J., J. A. Pyle, G. D. Carver, X. Yang, N. H. Savage, F. M. O'Connor, and R. A.
1027 Cox: Global modeling of biogenic bromocarbons, *J. Geophys. Res.*, 111, D24305,
1028 doi:10.1029/2006JD007264, 2006.

1029

1030 Wuebbles, D. J.: Chlorocarbon emission scenarios: Potential impact on stratospheric ozone,
1031 *J. Geophys. Res.*, 88, 1433–1443, 1983.

1032

1033 Wuebbles, D. J., K. Patten, M. Johnson, and R. Kotamarthi: New methodology for ozone
1034 depletion potentials of short-lived compounds: n-propyl bromide as an example, *J. Geophys.*
1035 *Res.*, 106, 14551–14571, 2001.

1036

1037 Yang, X., Abraham, N. L., Archibald, A. T., Braesicke, P., Keeble, J., Telford, P. J.,
1038 Warwick, N. J., and Pyle, J. A.: How sensitive is the recovery of stratospheric ozone to
1039 changes in concentrations of very short-lived bromocarbons?, *Atmos. Chem. Phys.*, 14,
1040 10431-10438, doi:10.5194/acp-14-10431-2014, 2014.

1041

1042 Ziska, F., Quack, B., Abrahamsson, K., Archer, S. D., Atlas, E., Bell, T., Butler, J. H.,
1043 Carpenter, L. J., Jones, C. E., Harris, N. R. P., Hepach, H., Heumann, K. G., Hughes, C.,
1044 Kuss, J., Krüger, K., Liss, P., Moore, R. M., Orlikowska, A., Raimund, S., Reeves, C. E.,
1045 Reifenhäuser, W., Robinson, A. D., Schall, C., Tanhua, T., Tegtmeier, S., Turner, S., Wang,
1046 L., Wallace, D., Williams, J., Yamamoto, H., Yvon-Lewis, S., and Yokouchi, Y.: Global sea-
1047 to-air flux climatology for bromoform, dibromomethane and methyl iodide, *Atmos. Chem.*
1048 *Phys.*, 13, 8915-8934, doi:10.5194/acp-13-8915-2013, 2013.

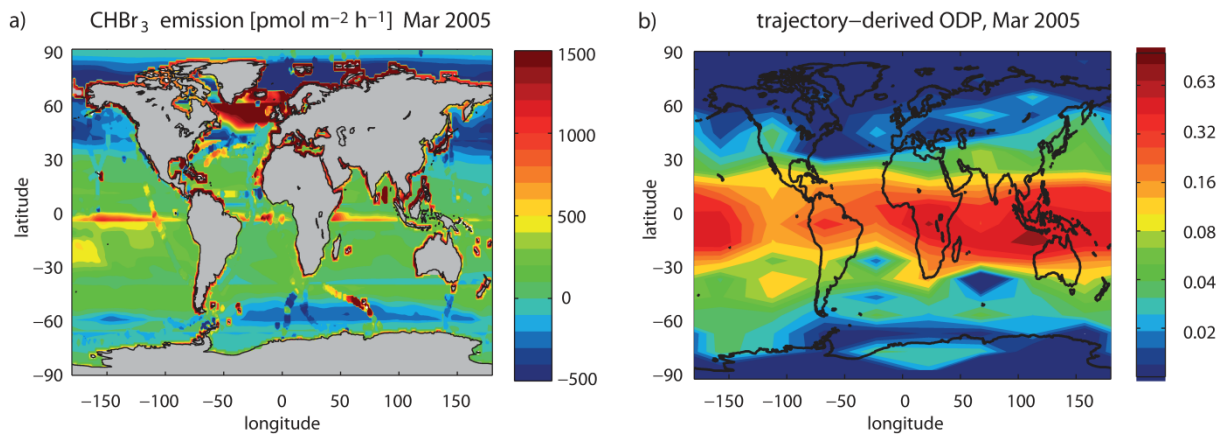
1049

1050 **Ziska, F., Quack, B., Krüger, K., and Tegtmeier, S.: Future emissions of halocarbons**
1051 **based on CMIP 5 model output fields, to be submitted to ACPD.**

1052

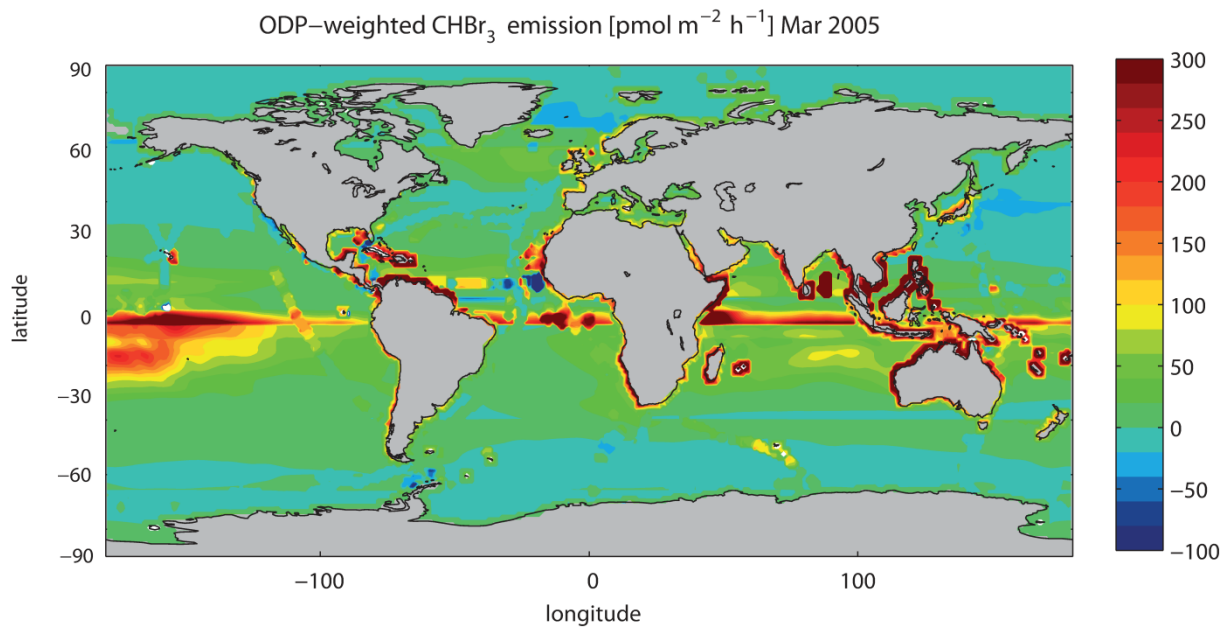
1053

1054



1055
 1056
 1057
 1058
 1059
 1060
 1061
 1062
 1063

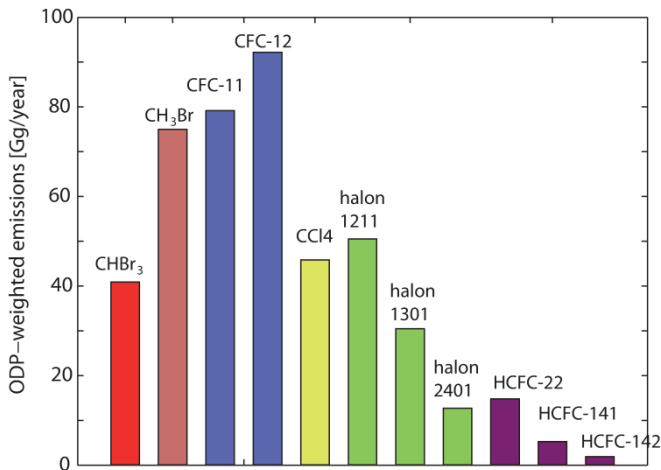
Figure 1. Global CHBr_3 emissions (a) and ODP (b) are given for March 2001. The CHBr_3 emissions are bottom-up estimates based on the extrapolation of in-situ measurements (Ziska et al., 2013). The ODP is given as a function of time and location of emission and was derived based on a Lagrangian approach (Pisso et al., 2010).



1064
 1065
 1066
 1067
 1068
 1069

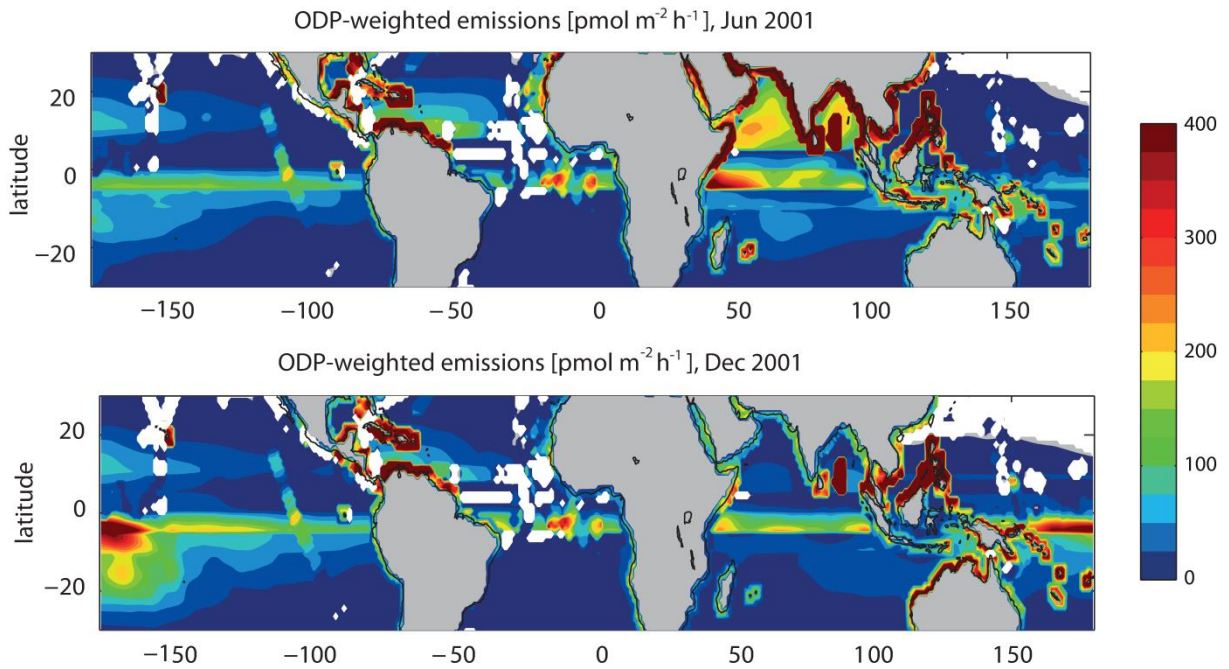
Figure 2. Global ODP-weighted CHBr_3 emissions are given for March 2005. The ODP-weighted emissions have been calculated by multiplying the CHBr_3 emissions with the ODP at each grid point.

Global annual mean ODP-weighted emissions, 2005



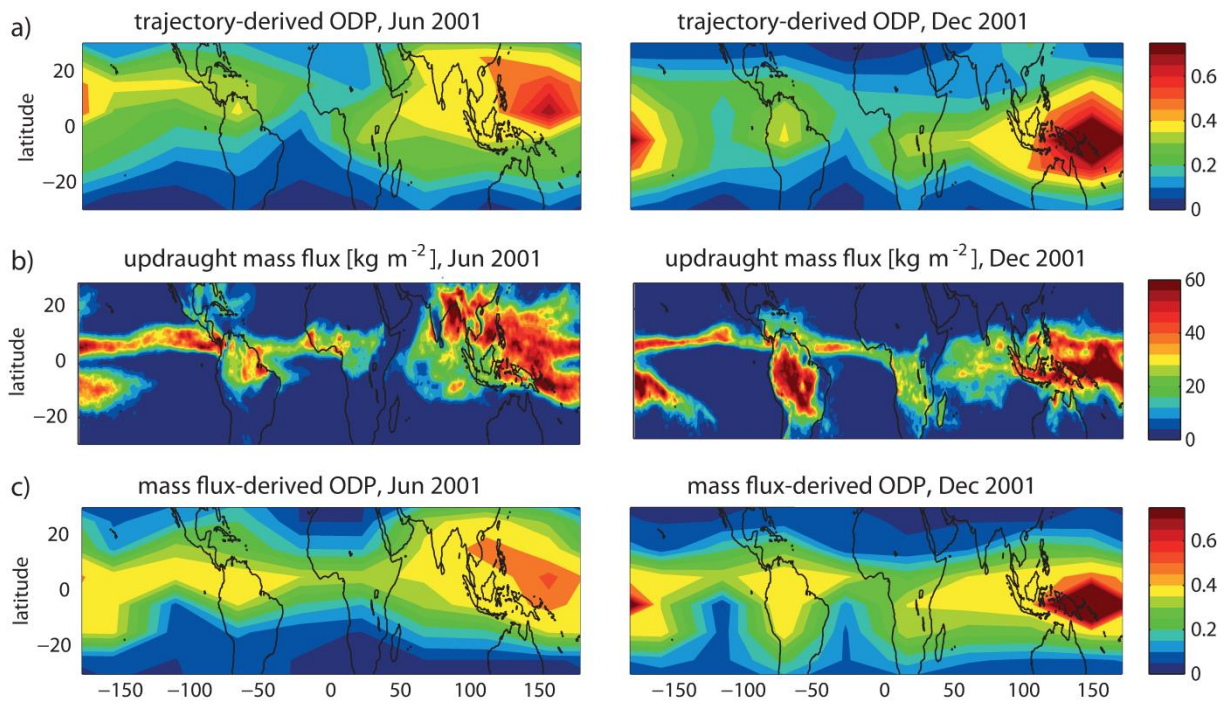
1070
1071
1072
1073
1074
1075
1076

Figure 3. A comparison of the global annual mean ODP-weighted emissions of CHBr₃ and long-lived halocarbons is shown for 2005. Emissions of long-lived halocarbons being derived from NOAA and AGAGE global sampling network measurements (Montzka et al., 2011).



1077
1078
1079
1080
1081
1082

Figure 4. ODP-weighted emissions calculated as the product of the emissions maps (not show here) and the trajectory-based ODP fields (Figure 5a) are displayed for June and December 2001.



1083

1084

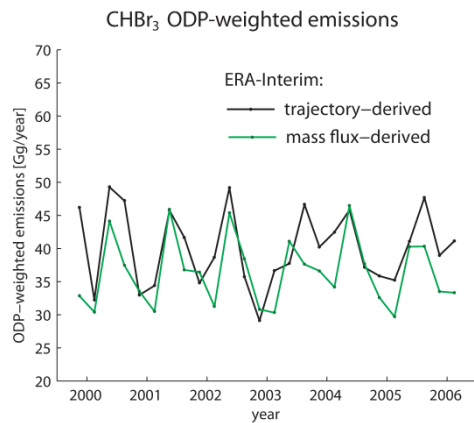
Figure 5. Trajectory-based CHBr₃ ODP fields (a), monthly mean ERA-Interim updraught mass flux between 250 and 80 hPa (b), and the mass flux-derived ODP (c) are displayed for June and December 2001.

1085

1086

1087

1088



1089

1090

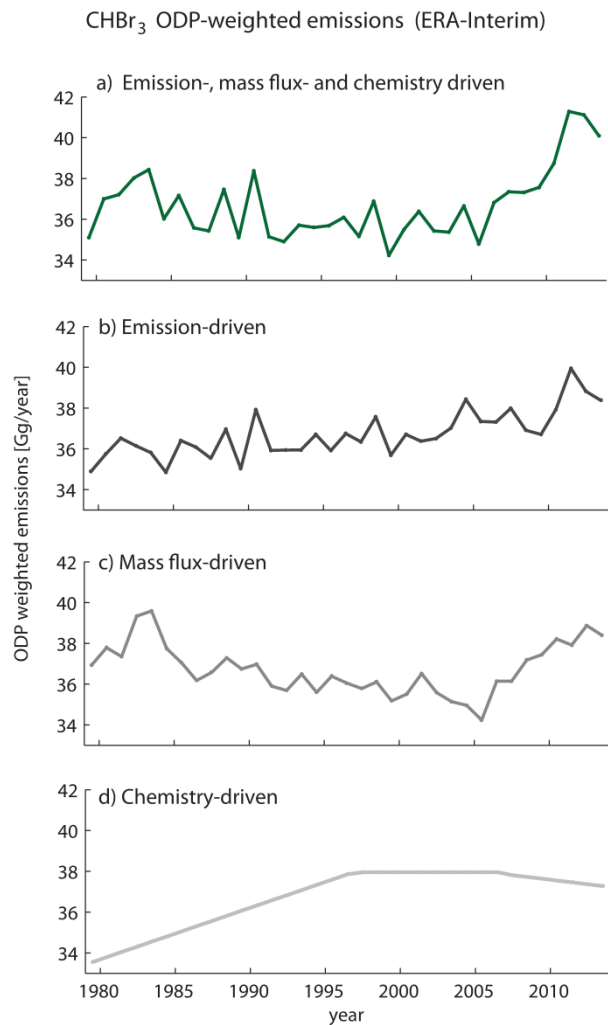
Figure 6. Time series of ODP-weighted CHBr₃ emissions based on ERA-Interim trajectory-derived ODP (black line) and mass flux-derived ODP (green line) for March, June, September and December 1999 to 2006.

1091

1092

1093

1094



1095

1096

1097

1098

1099

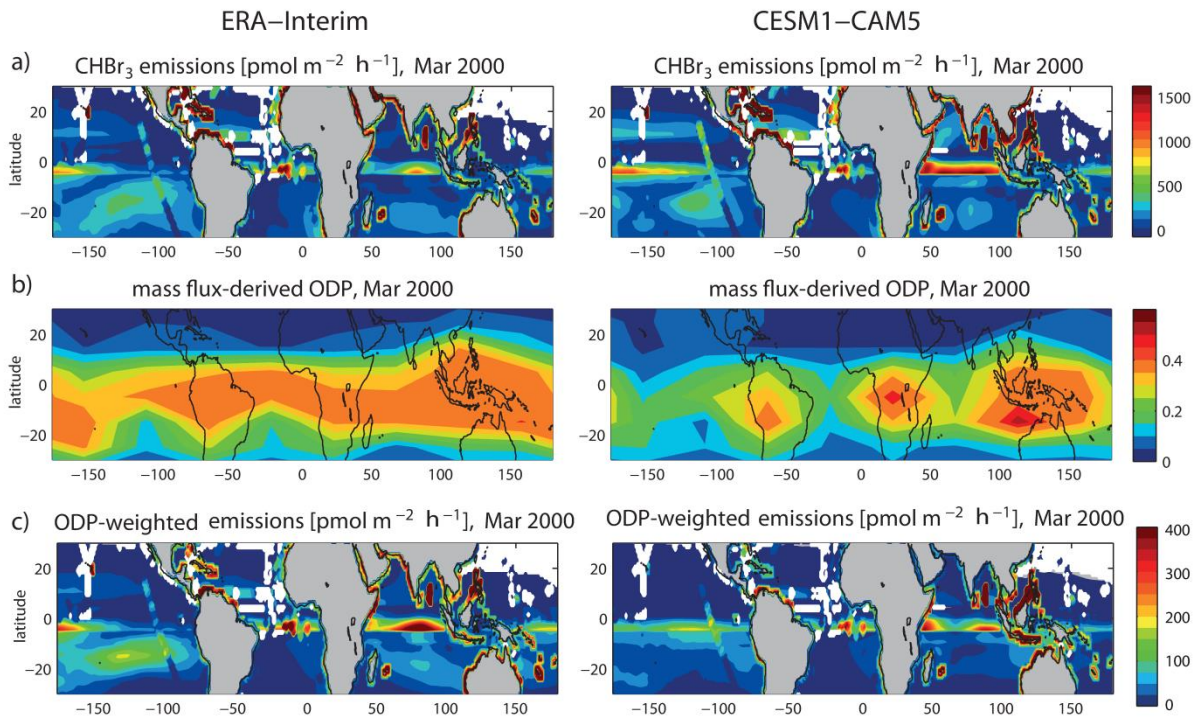
1100

1101

1102

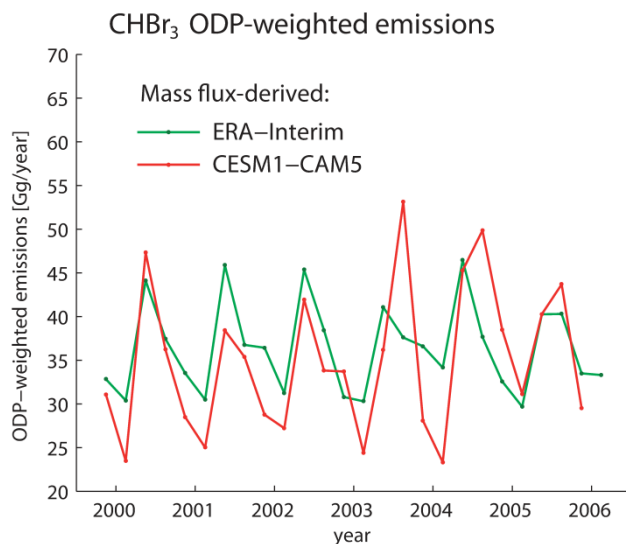
1103

Figure 7. Time series of ODP-weighted CHBr₃ emissions for 1979-2013 based on ERA-Interim mass flux-derived ODP is shown (a). Additionally, sensitivity studies are displayed where two factors are kept constant at their respective 1979-2013 mean values, while the other factor varies with time. The sensitivity studies include ODP-weighted CHBr₃ emissions driven by time-varying emissions (b), time-varying mass flux-derived ODP (c), and time-varying stratospheric chemistry (d).



1104
1105
1106
1107
1108
1109

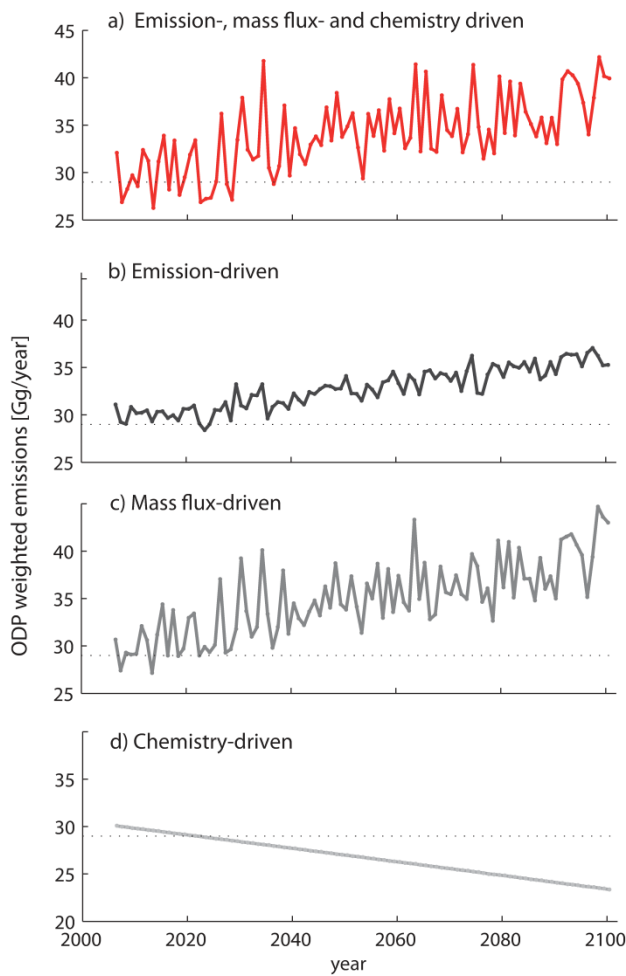
Figure 8. CHBr₃ emissions (a), mass flux-derived ODP (b) and ODP-weighted CHBr₃ emissions (c) are shown for ERA-Interim and for CESM1-CAM5 for March 2000.



1110
1111
1112
1113
1114
1115
1116

Figure 9. Time series of CHBr₃ ODP-weighted emissions based on ERA-Interim (green line) and on historical CESM1-CAM5 runs (red line) are shown. The ODP is calculated from the updraught mass flux fields.

CHBr₃ ODP-weighted emissions (CESM1-CAM5)



1117

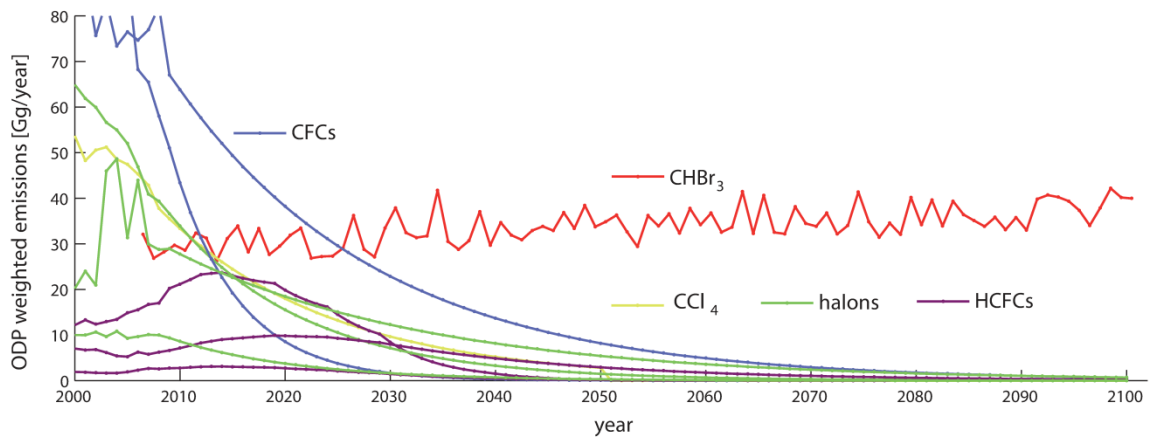
1118

1119 **Figure 10.** Time series of CHBr₃ ODP-weighted emissions for 2006-2100 based on future (RCP 8.5
1120 scenario) CESM1-CAM5 runs are shown (a). Additionally, the future time series are displayed with
1121 two factors kept constant at their respective 2006-2015 mean value while the other factor varies with
1122 time. The sensitivity studies include ODP-weighted CHBr₃ emissions driven by time-varying
1123 emissions (b), time-varying mass flux-derived ODP (c), and time-varying stratospheric chemistry (d).

1124

1125

1126



1127

1128 **Figure 11:** Future projections of annual mean ODP-weighted emissions of CHBr₃ and other long-lived
 1129 halocarbons are shown for 2000-2100. Future ODP-weighted emission estimates for long-lived
 1130 halocarbons (halons: halon 1211, 1301, 2402; HCFCs: HCFC-22, -141, -142) are shown.

1131